J. Fish. Sci. Tech. 4(3), 101~111, 2001

JOURNAL OF
FISHERIES SCIENCE
AND TECHNOLOGY

A Geostrophic Adjustment Model of the Seasonal Variation of the Ulleung Warm Eddy

Young Ho Seung

Dept. of Oceanography, Inha University, Inchon 402-751, Korea

(Received June 2001, Accepted September 2001)

In an attempt to demonstrate the seasonal variation of the Ulleung Warm Eddy (UWE), in which the UWE changes its shape from a warm core ring in early spring to a warm lens in late summer under the effect of surrounding East Korean Warm Current (EKWC) Water, a simple geostrophic adjustment model is considered. Model results indicate that the buoyancy increase of the EKWC Water and the strengthening of the EKWC towards summer, both of which are typical of this region, are the major factors governing the seasonal variation of the UWE.

Key words: Ulleung Warm Eddy, Geostrophic adjustment

Introduction

Since the investigation initiated by Uda (1934), the surface circulation in the East Sea has been known to be as follows. The Tsushima Warm Current enters the East Sea through the Korea Strait. It then bifurcates into two distinct branches - an eastern branch called the Nearshore Branch (briefly, NB) flowing along the Japanese coast and a western branch called the East Korean Warm Current (briefly, EKWC) flowing along the Korean coast (Fig. 1). The EKWC separates from the coast where it meets the southward flowing Liman Current (briefly, LC) or North Korean Cold Current (briefly, NKCC). Thereafter, both currents flow, on average, eastward forming the subpolar front between them. However, the detailed flow pattern seems to be very complicated involving many eddies and meanders as suggested by drifter experiments (Lie et al., 1995). Both the EKWC and the NB flow out either to the Pacific through the Tsugaru Strait or to the Okhotsk Sea through the Soya Strait, but the LC or the NKCC recirculates around the basin north of the subpolar front. The overall characteristics of the East Sea circulation pattern described above (Fig. 1) is relatively well supported by many numerical experiments (e.g., Seung and Kim, 1993; Kim and Yoon, 1999). The main features of the EKWC and NB described above are well reflected by the horizontal temperature distribution at depth 100 m (Fig. 2). It has been known that the EKWC is formed by the beta-effect (Yoon, 1982), and the NB is a Kelvin wave manifestation of the buoyancy change at the inflow opening of the basin, i.e., at the Korea Strait, whereas the LC or the NKCC has been believed to be generated by local wind and buoyancy forcings (e.g., Seung, 1992; Kim and Seung, 1999).

Among the various currents mentioned above, special attention is paid to the EKWC. It passes through the western part of the Korea Strait, i.e., between Busan and Tsushima (Fig. 1). Its transport is known to be maximum in summer and minimum in winter as estimated by the sea level difference between Busan and Tsushima (Yi, 1966). The EKWC Water is characterized by its high-salinity and high-temperature originating from the Kuroshio, the western boundary current of the North Pacific (Moriyasu, 1972). This character is substantially reduced in winter but is recovered rapidly afterwards. The anti-cyclonic behavior of the EKWC

*Corresponding author: seung@inha.ac.kr

after separation from the coast, which has not been drawn much attention, is of special interest. This behavior is depicted in the schematic chart by the branching of the EKWC toward the NB just after separation (Fig. 1), in the historical temperature distribution at depth 100 m by the southward bending of the 5~9℃ isotherms (Fig. 2), and in the infrared satellite image by the warm streamer of the EKWC Water almost completing a circle (Plate 1). Especially, this satellite image indicates that a significantly large amount of the EKWC Water circulates around the UWE. Part of it is thought to escape from the anti-cyclonic circulation before completing the circular trajectory, to join the mainstream of the EKWC.

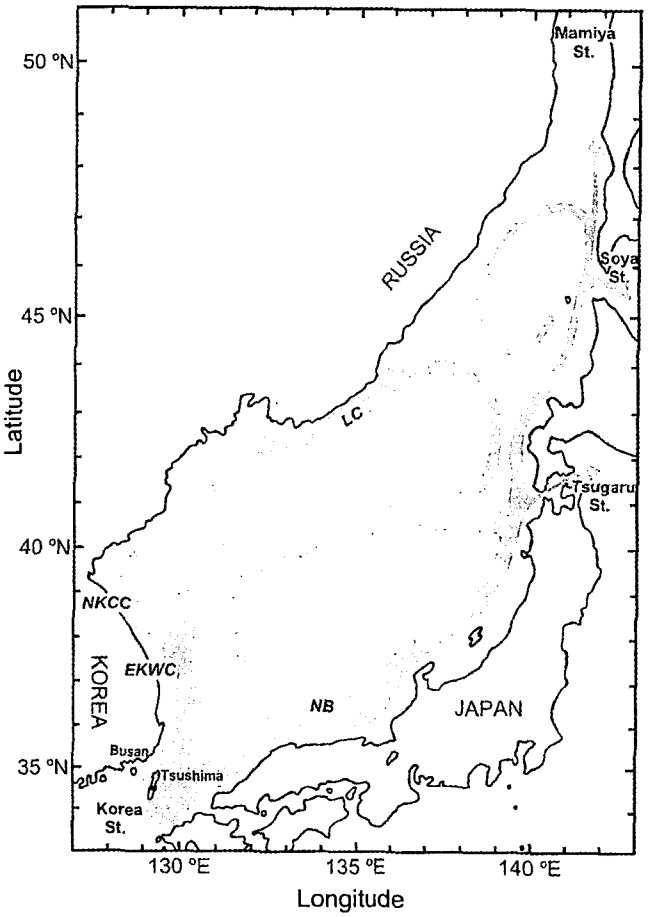

Fig. 1. Schematic diagram showing the surface circulation pattern of the Japan/East Sea with East Korean Warm Current (EKWC), Liman Current (LC), North Korean Cold Current (NKCC) and Nearshore Branch (NB). (after Senjyu, 1999)

The anti-cyclonic behavior of the EKWC seems to be linked to the presence of an isolated mass of warm water found at depths 100~300 m just off the separation point (Fig. 2). Since this water is centered, on average, near Ulleung Island (37.4°N, 130.8° E), it is often called Ulleung Warm Eddy (briefly, UWE). Actually, however, the position of the UWE has been known to change from time to time around its average position (Kang and Kang, 1990). The UWE water has been believed to owe its warm and saline character to the overlying EKWC Water which is mixed downward by winter convection (Kim, 1991). In most cases, however, these findings were based on the temperature data obtained at relatively sparsely distributed observation points along zonal directions, and detailed measurements of the UWE had been required.

Recent observations in 1992 and 1993 have revealed the detailed structure of the UWE and its seasonal variation (KORDI, 1993 and 1994; Shin et al., 1995). In these observations, the entire UWE is relatively well homogenized in early spring with little EKWC Water at the surface (Fig. 3), showing the shape of a warm core ring, which otherwise has the shape of a lens most of the time. As the season progresses towards summer, the UWE becomes more surrounded by the EKWC Water, and an appreciable amount of the EKWC Water moves into the upper portion of the UWE, overriding the latter. Finally, in late summer, the UWE becomes lens-shaped under the effect of the EKWC Water (Fig. 3). The UWE thus deformed will be renewed again by cooling-induced vertical mixing in coming winter, hence completing the annual cycle.

The aim of this paper is to extract major factors governing the seasonal variation of the UWE, using a simple analytic model. This paper is structured as follows. In section 2, a simple analytical model is formulated and in section 3, the model results are analysed and interpreted. Finally in section 4, some discussion is offered and conclusions are presented.

Model formulation

To demonstrate the seasonal variation of the UWE described in the previous section, a simple analytical model is constructed by idealizing the

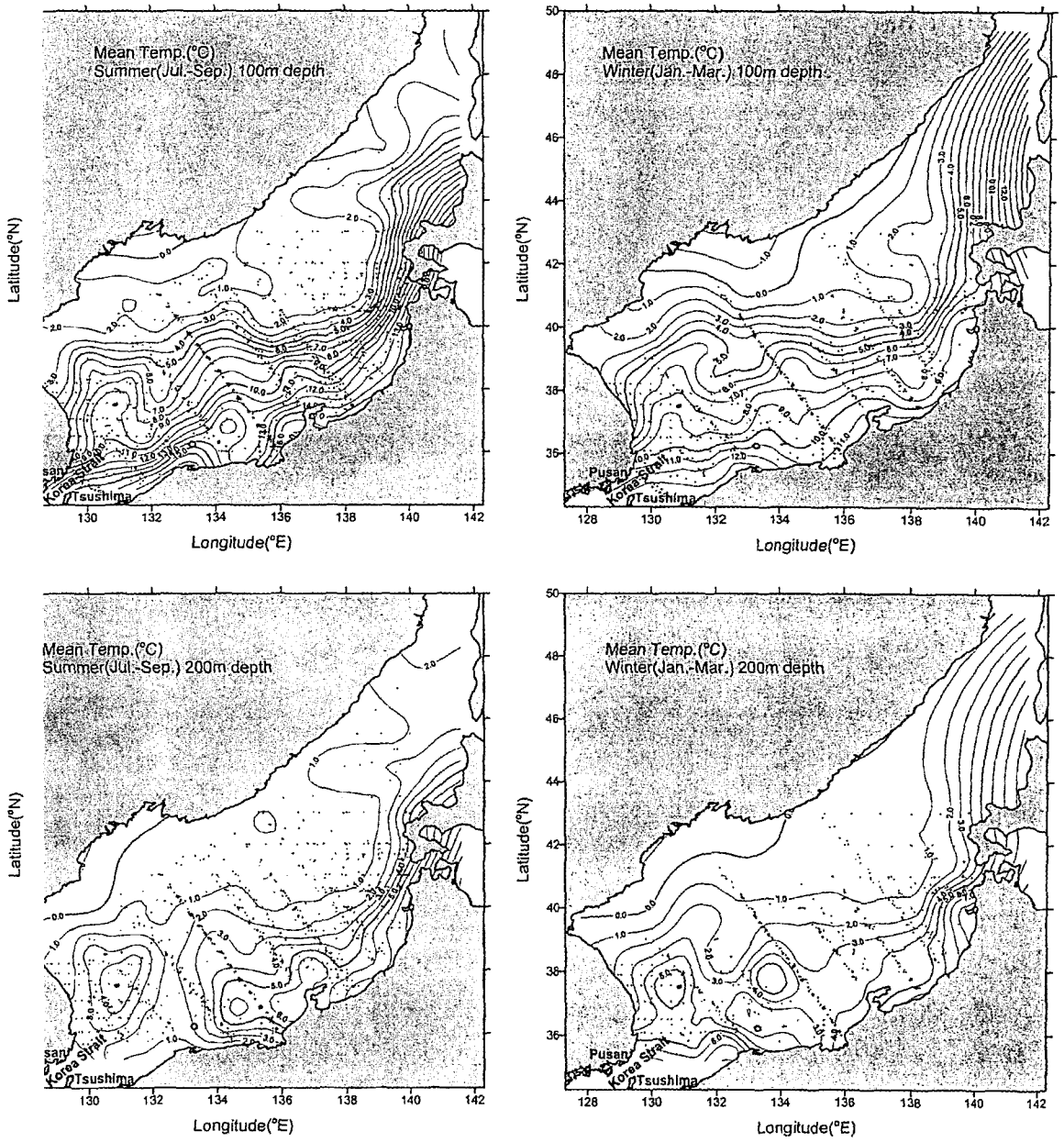

Fig. 2. Summer and winter mean temperatures at depths 100 m and 200 m constructed based on the historical data from Maizuru Marine Observatory, Japan and National Fisheries Research and Development Agency, Korea.

problem as described below. Consider a two-layer ocean on an f-plane bordering a meridional boundary to the west (upper part of Fig. 4). In the upper layer, an inertial boundary current flows along the meridional boundary, overlying the lower motionless layer. Here, the meridional boundary may also be considered as the outer edge of the EKWC. Consider an anti-cyclonic eddy embedded near the offshore edge of the boundary current. This eddy is filled with homogeneous water of density intermediate between those of the upper and lower layers of the model ocean; the eddy is thick enough to be outcropped to the surface. Around the eddy, a significant portion of the boundary current is trapped circulating anti-cyclonically, which is referred to as the "trapped" boundary current. Outside the trapped

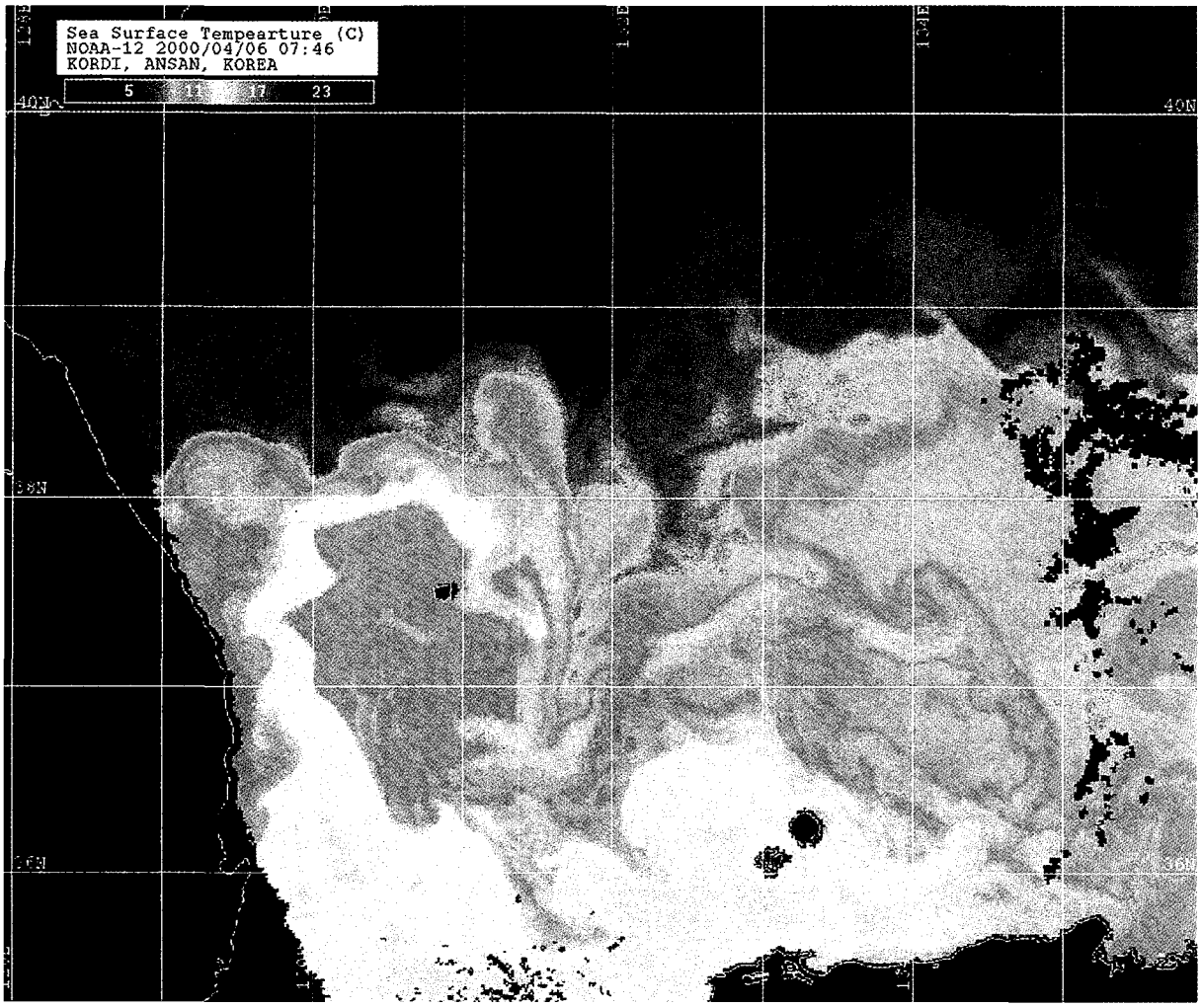

Plate 1. Surface temperature distribution obtained from the NOAA-12 AVHRR infrared image on LT 07:46 in April 6, 2000. Grid lines (white) represent one degree of latitude and longitude (courtesy of KORDI).

boundary current, the remainder of the boundary current continues to flow along the boundary, which is referred to as the "free" boundary current. Here, the eddy mimics the UWE; the free boundary current, the portion of the EKWC which passes by the UWE along its mean direction; and the trapped boundary current, the portion of the EKWC anticyclonically circulating around the UWE. The process associated with the trapping of the EKWC around the UWE is yet an unanswered problem, and will not be pursued here. Based on the observations (KORDI, 1993 and 1994; Shin et al., 1995), assume that the free boundary current is negligibly weak compared to the trapped boundary current such that conditions become axi-symmetric around the eddy center. Let the densities of the upper and lower layers of the model ocean be constant at ρ_1 and ρ_3, respectively, and that of the water within the eddy, at ρ_2. All three water bodies (named first, second and third layers following the subscript numbers) are assumed to be inviscid and hydrostatic, and to conserve their potential vorticities. Actually, the EKWC Water circling around the UWE differs from the neighboring water in the same layer, and can be differentiated by its higher salinity and higher temperature (cf., Fig. 3). However, the densities of these two waters are so close to each other relative to the density of the UWE water that they can be treated the same.

The three water bodies are stable only when they are geostrophically balanced. This can be achieved through the geostrophic adjustment by releasing the

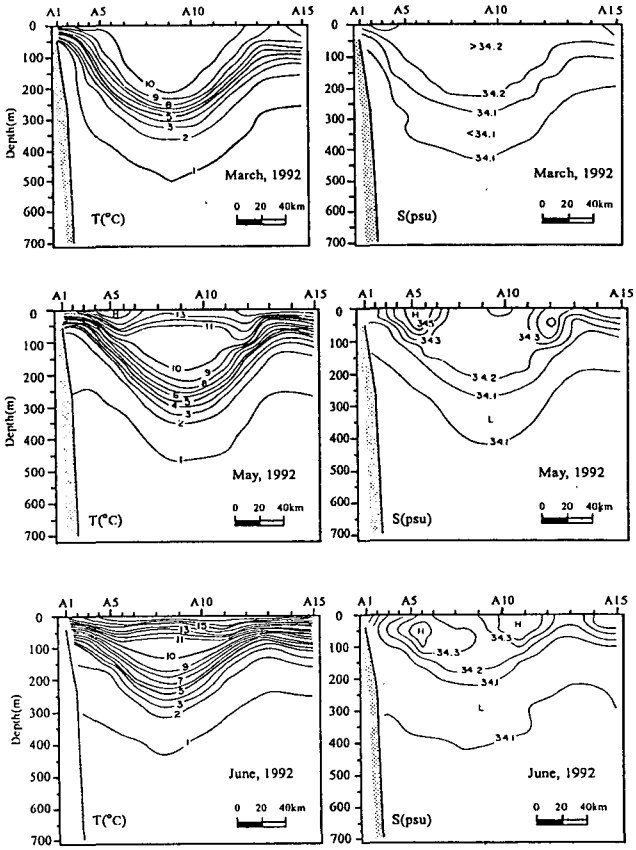

Fig. 3. Temporal evolution of the UWE structure on the zonal section A (approximately along 38.2°N, station numbers increasing eastward) crossing the UWE center. (after Shin et al., 1995)

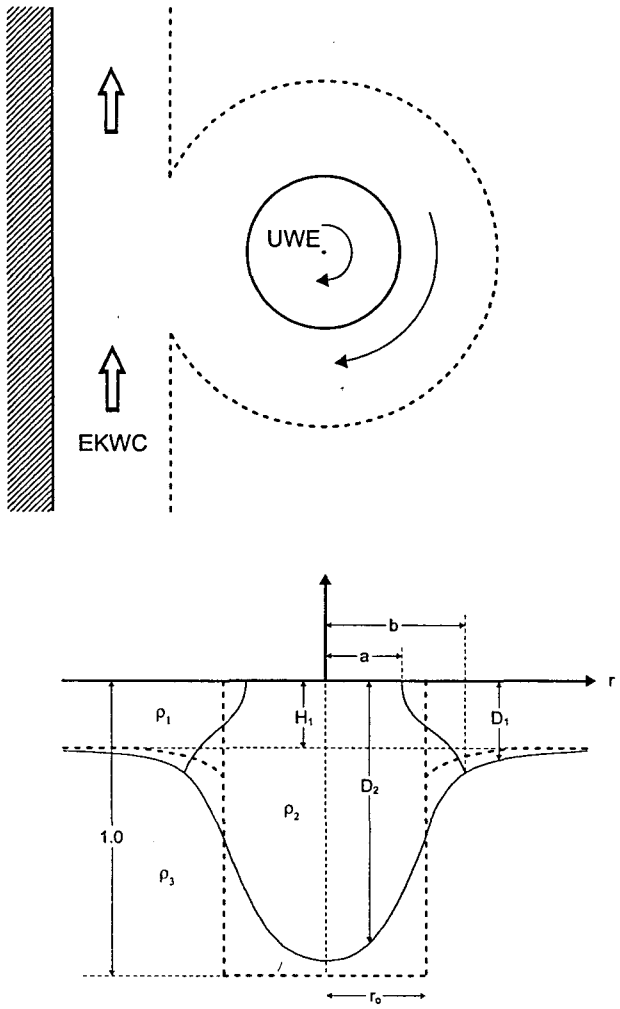

Fig. 4. Upper: Schematic plan view idealizing the UWE enclosed by the anti-cyclonically circulating EKWC. The remainder of the EKWC continues to flow along the boundary. The solid circle and the dotted line denote the boundaries of the outcropped UWE and of the area dominated by the EKWC, respectively. Lower: Vertical section of the idealized UWE and the surrounding EKWC Water, across the UWE center. Thick dotted lines and thin solid lines denote, respectively, the initial and final states with respect to the geostrophic adjustment. The thickness of the UWE in the initial resting state is taken as the unity.

water bodies from an arbitrary initial state in which they can be gravitationally unstable but have to conserve their potential vorticities and volumes initially given to them. The problem is solved by finding the final steady state. In our case, we assume an initial state where the eddy is motionless and of cylindrical form. Around this eddy, the first layer circulates anti-cyclonically with an initially given speed. It is legitimate to assume the initially motionless eddy because the final kinetic energy of the eddy is extracted internally from the potential energy of the initial eddy during the adjustment process. However, this is not the case for the initial current of the first layer because the EKWC is initially given externally although it is modified later by the adjustment. Hence, the initially-given speed of the anti-cyclonic component of trapped boundary current, which is v_0 at the edge of the cylindrical eddy, is proportionately dependent on the strength of the EKWC. The mathematical expression of this initial state, though not given here, can be obtained from the equations of geostrophic relationship and the conservation of the potential vorticity, as becomes clear later. In the initial state, the layer thickness

and speed of the anti-cyclonic component of the trapped boundary current, both expressed in terms of v_0, decrease radially outward to reach those in a resting state infinitely far from the eddy. In the final state after completing the geostrophic adjustment, a mutual intrusion between the first and second layers is expected with the former overriding the latter. The interface between them slopes upward toward the eddy center, resulting in the deformation of the eddy (lower part of Fig. 4). Although it is expected that the deformation is further enhanced by local mixing and diffusion, these are not considered in this model. As a result of the geostrophic adjustment, currents are induced within the eddy and the initial current of the first layer is modified.

Take the cylindrical coordinate with azimuthal angle increasing in the counter- clockwise direction, radial distance r increasing away from the origin taken at the center of the eddy, and vertical axis taken positively upward. Although, in actual situations, the eddy changes its position by interaction with the mean and trapped boundary currents, we confine our attention only to the vicinities of the eddy by moving with the eddy. For convenience, non-dimensionalize the thickness variables by H_2 - the potential thickness of the eddy (thickness in resting state), the horizontal distance variables by the Rossby radius $R=\sqrt{g'H_2}/f$ (g' is the reduced gravity between the second and third layers, and f is the Coriolis' parameter), and the velocity variables by fR. Hereafter, all these variables are understood as non-dimensionalized unless otherwise stated. The governing equations are the potential vorticity conservations:

$$\frac{1}{H_1} = \frac{1+v_1/r+dv_1/dr}{D_1} \tag{1}$$

$$1 = \frac{1+v_2/r+dv_2/dr}{D_2} \tag{2}$$

for the first and second layers, respectively, where v is the azimuthal component of velocity, D is the layer thickness with the subscript number denoting the layer considered, and H_1 is the potential thickness (non-dimensional thickness in the resting state) of the first layer (lower part of Fig. 4). The geostrophic relationships have different expressions depending on the domains considered. For the domain r>b, where b is the radial position of the outer edge of the eddy (lower part of Fig. 4), it is

$$v_1 = \Delta_3 dD_1/dr \tag{3}$$

where $\Delta_3=(\rho_3-\rho_1)/(\rho_3-\rho_2)$. For the domain a<r<b, where a is the position of the inner edge of the first layer, it is

$$v_1 - v_2 = \Delta_2 dD_1/dr \tag{4}$$

where $\Delta_2=(\rho_2-\rho_1)/(\rho_3-\rho_2)$. For the domain 0<r<a, it is

$$v_2 = dD_2/dr \tag{5}$$

General solutions are found using a method similar to that used by Seung (1999). For the domain r>b, elimination of v_1 from (1) and (3) leads to a second order ordinary differential equation in terms of only D_1, which has the solution

$$D_1 = H_1 + c_1 I_0(\beta r) + c_2 K_0(\beta r) \tag{6}$$

where I_0 and K_0 are the modified Bessel functions of zero order of the first and second kinds, respectively, $\beta=1/\sqrt{\Delta_3 H_1}$, and c_1 and c_2 are unknown constants. It will be shown later that for (6) to have finite values at infinitely large r, the terms involving I_0 should be eliminated. Introducing (6) to (3) gives v_1:

$$v_1 = c_1 \Delta_3 \beta I_1(\beta r) - c_2 \Delta_3 \beta K_1(\beta r) \tag{7}$$

Likewise, for the domain a<r<b, (1), (2), (4) and (5) lead to

$$D_1 = H_1 + c_3 I_0(\alpha_1 r) + c_4 K_0(\beta_1 r) + c_5 I_0(\alpha_2 r) + c_6 K_0(\alpha_2 r), \tag{8}$$

$$D_2 = 1 + (1/H_1 - \Delta_2 \alpha_1^2)[c_3 I_0(\alpha_1 r) + c_4 K_0(\alpha_1 r)] + (1/H_1 - \Delta_2 \alpha_2^2)[c_5 I_0(\alpha_2 r) + c_6 K_0(\alpha_2 r)], \tag{9}$$

$$v_1 = \alpha_1(1/H_1 - \Delta_2 \alpha_1^2 + 1 + \Delta_2)[c_3 I_1(\alpha_1 r) - c_4 K_1(\alpha_1 r)] + \alpha_2(1/H_1 - \Delta_2 \alpha_2^2 + 1 + \Delta_2)[c_5 I_1(\alpha_2 r) - c_6 K_1(\alpha_2 r)], \tag{10}$$

$$v_2 = \alpha_1(1/H_1 - \Delta_2 \alpha_1^2 + 1 + \Delta_2)[c_3 I_1(\alpha_1 r) - c_4 K_1(\alpha_1 r)] + \alpha_2(1/H_1 - \Delta_2 \alpha_2^2 + 1)[c_5 I_1(\alpha_2 r) - c_6 K_1(\alpha_2 r)] \tag{11}$$

where c_3 through c_6 are unknown constants and

$$\alpha_1,\ \alpha_2 = \left[\frac{(\Delta_2+1+1/H_1) \pm \sqrt{\Delta_2+1+1/H_1)^2 - 4\Delta_2/H_1}}{2\Delta_2}\right]^{1/2}$$

For the domain 0<r<a, (2) and (5) lead to

$$D_2 = 1 + c_7 I_0(r) + c_8 K_0(r), \tag{12}$$

$$v_2 = c_7 I_1(r) - c_8 K_1(r) \tag{13}$$

where c_7 and c_8 are unknown constants. The 8 unknown constants, c_1 through c_8, together with a and

b are determined by applying the ten conditions to be satisfied. These conditions are:

1) boundedness of solutions at infinitely large r
2) continuity of D_1 at r=b
3) continuity of v_1 at r=b
4) continuity of D_2 at r=a
5) continuity of v_2 at r=a
6) $v_2=0$ at r=0
   (symmetry of solutions about r=0)
7) $D_1=0$ at r=a
8) $D_2=0$ at r=b
9) $v_1=-v_0+(r_0-a)$ at r=a
10) $v_2=-(b-r_0)$ at r=b

where ro is the radius of the cylindrical eddy in the initial state (lower part of Fig. 4) and v_0 (>0) is the initial speed of the first layer at $r=r_0$ measured anticyclonically. A special note is required for conditions 9) and 10). They describe the relationship between the radial excursion experienced by a particle, occurring during the adjustment, and the azimuthal component of velocity it acquires in the final state. This is due to the Coriolis' effect and the corresponding relationship can be obtained by time-integrating the azimuthal component of the momentum equation in the Lagrangian sense (cf., Seung, 1999). Moreover, the condition 10) is equivalent to the requirement that the volume of the eddy is conserved.

Model results

The ten conditions, 1) through 10), are applied to the general solutions, (6) through (13), and are solved numerically using IMSL routine for specific values of parameters H_1, ρ_1 through ρ_3, r_0 and v_0. The use of fixed values for these parameters, which otherwise may change seasonally, can be justified by the fact that the geostrophic adjustment process takes place nearly instantaneously compared to the seasonal variation of these parameters. Observations (eg., Fig. 3) indicate that the densities ρ_2 and ρ_3 do not change appreciably with time compared to ρ_1; and are treated as constants with the values, 1.0263 and 1.0273, respectively. Likewise, the potential thickness of the upper layer H_1, and the volume of the eddy r_0, do not change appreciably, at least over the period of a year after having been determined in winter (cf., Fig. 3), and are fixed at typical values of 0.3 and 3.0, respectively. In dimensional unit, these values are approximately 100 m and 52 km, respectively, for dimensional $H_2=300$ m, $f=10^{-4}\,sec^{-1}$ and $g'=10^{-2}\,m/sec^2$. On the contrary, the surface water including the EKWC Water suffers large seasonal effects and the transport (or velocity) of the EKWC is known to undergo large seasonal fluctuation. Therefore, ρ_1 and v_0 are considered here to be the major parameters governing the seasonal change of the UWE structure.

The density ρ_1 decreases greatly towards summer due partly to the surface heating and partly to the advection of low-density water by the EKWC (Fig. 3). The latter fact is evident because the density of the EKWC Water upstream of the UWE area, i.e., across the line connecting Busan and Tsushima, decreases rapidly between winter and summer (Fig. 5). There, the density ρ_1 appears slightly smaller than that near the UWE because of the local modification that the EKWC Water undergoes between the two areas. For instance, the EKWC Water in June 1992 (Fig. 3) has density larger than 25.5 (in sigma-t unit) for temperature 10~15℃ and salinity 34.3~34.5 psu whereas, during the same period, that in the Korea Strait (Fig. 5) has density slightly smaller than 24.3. Informations about the initial velocity v_0 are hard to obtain from observed currents because they have already been modified by geostrophic adjustment. Since v_0 is proportionately linked

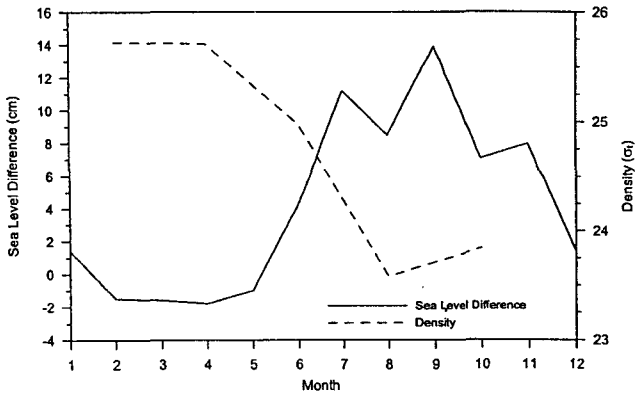

Fig. 5. Monthly mean values of sea level difference between Busan and Tsushima and of sea water density spatially averaged between the two locations in upper 100 m, observed in 1992. See Figure 1 for locations.

to the strength of the EKWC, its time variation can be estimated by knowing the time-change of sea surface slope across Busan and Tsushima (see Fig. 1 for location). Indeed, a large increase of the sea level difference is apparent between winter and summer (Fig. 5). In subsequent analyses, therefore, we consider values ranging from 1.02505 to 1.02615 for ρ_1 and from 0 to 1.0 for v_0.

Solutions obtained for these ρ_1 and v_0 show density structures comparable to those observed (eg., Fig. 6). Velocities both inside the eddy and in the first layer increase rapidly in the radial direction until they reach a maximum near the outer edge of the eddy, thereafter the velocity in the first layer decreases radially outwards. This pattern resembles that of the velocities observed near the UWE (Fig. 7, 16 and 20 of Shin et al., 1995). However, the model fails to reproduce some detailed structures of the observations. For instance, it shows a two-layer structure in the area where both the first and second layers are present ($a<r<b$), which is not seen in observations. It also happens in the model that the current near the edge of the first layer reverses its direction, giving rise to a large vertical shear. This is induced by large inward excursion experienced by the water particles found near the edge of the first layer. All these discrepancies seem to arise from the fact that the model neglects the shear-induced vertical mixing, as discussed more later.

The variables a, b, D_2 at $r=0$, and v_1 at $r=a$, which represent the structures of the eddy and the surrounding first layer, are evaluated as functions of ρ_1 and v_0. The radial position of the first layer edge, a, decreases with v_0 and increases with ρ_1, meaning that the inward intrusion of the first layer develops towards summer (Fig. 7). Dynamically, the dependence of the intrusion on ρ_1 and v_0 can be explained as follows. The vertical boundary between two water bodies becomes gravitationally more unstable as the density difference between them increases, i.e., as ρ_1 decreases, hence increasing the tendency of mutual intrusion. Positive vertical shear (velocity increasing upward) develops as the mutual intrusion associated with the geostrophic adjustment proceeds until finally the thermal wind relationship is satisfied. Hence, the intrusion can proceed farther if the adjustment starts with a smaller initial vertical shear, i.e., with a larger anti-cyclonic velocity v_0. The

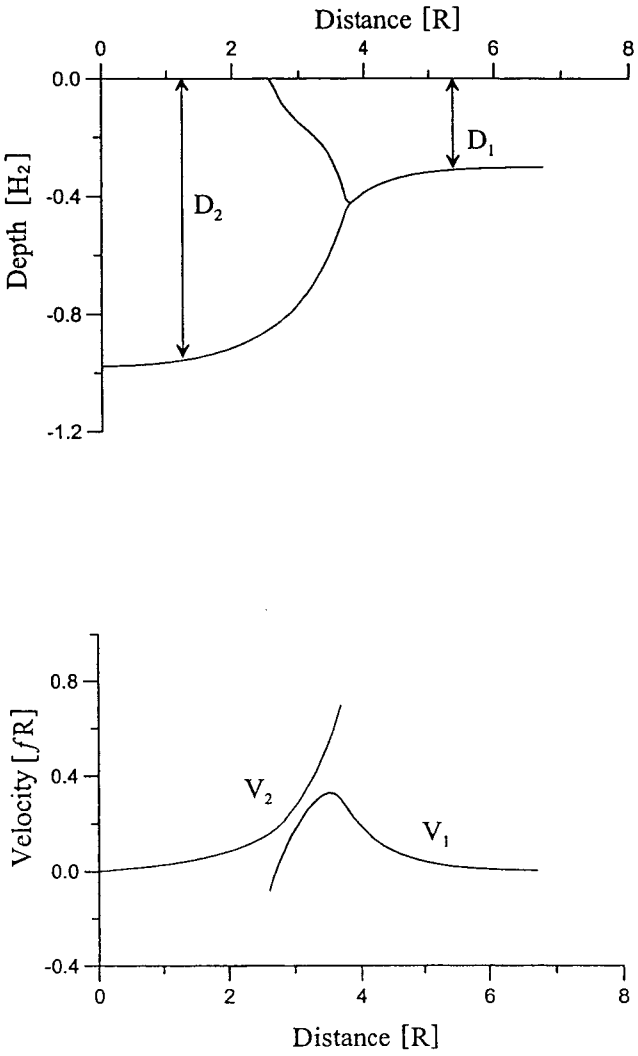

Fig. 6. Upper: Vertical structure of the eddy (thickness D_2) and the first layer (thickness D_1) in the final state. Lower: Anti-cyclonic component of the current velocities in the first layer (v_1) and within the eddy (v_2). Distance is measured from the eddy center radially outward. Parameters in parentheses are normalization factors. Parameters used are $H_1=0.3$, $r_0=3.0$, $\rho_1=1.02585$, $\rho_2=1.0263$, $\rho_3=1.0273$ and $v_0=0.3$.

velocity at the edge of the first layer, v_1 (a), becomes more cyclonic towards summer, i.e., for stronger initial anti-cyclonic velocity, v_0, and for smaller first layer density, ρ_1 (Fig. 8). Thus, the cyclonic component of velocity acquired by a water particle during the intrusion greatly exceeds the anti-cyclonic component of velocity initially given to it. As a consequence of the mutual intrusion, the outward exten-

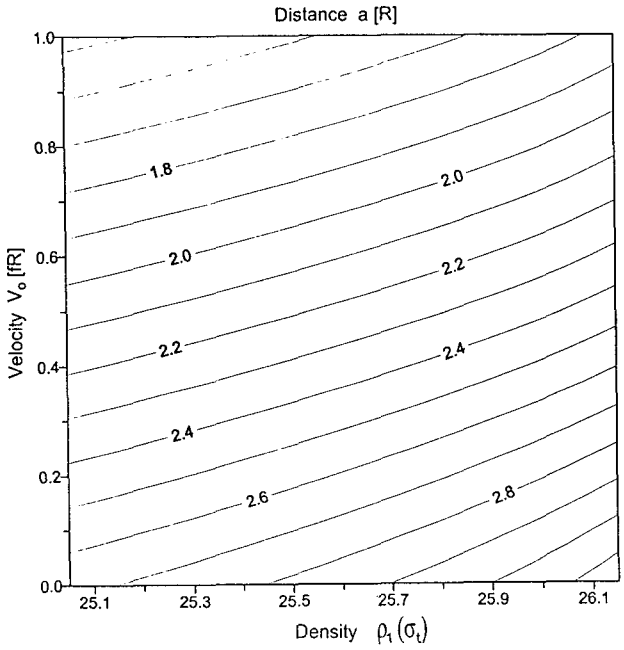

Fig. 7. Distances from the eddy center to the edge of the first layer, a, as functions of the initial anti-cyclonic component of velocity at $r=r_0$, v_0, and the first layer density ρ_1 (in sigma-t unit). Parameter in parentheses are normalization factors.

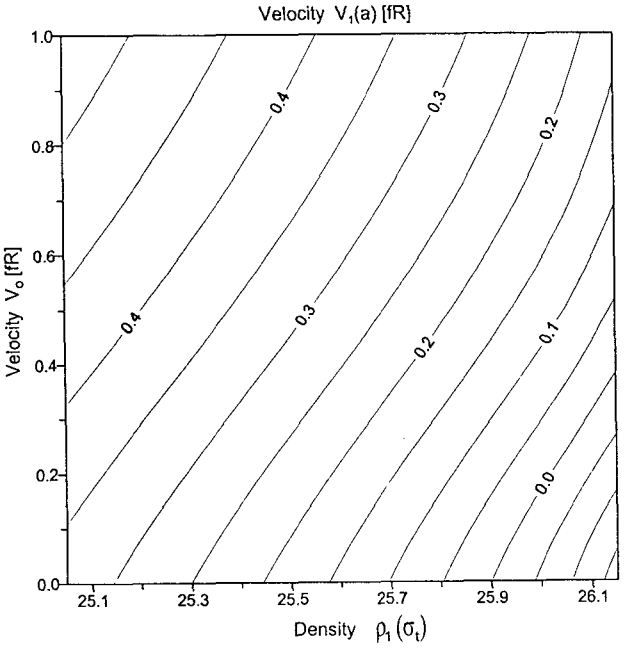

Fig. 8. Cyclonic component of the velocity, v_1, at the edge of the first layer, r=a. Others are the same as in Figure 7.

sion of the eddy develops towards summer, as seen from the behavior of b in response to v_0 and ρ_1 (Fig. 9). This is accompanied by a slight thinning of the eddy because the volume of the eddy has to be conserved, as seen from the behavior of D_2 (0) in response to v_0 and ρ_1 (Fig. 10). It follows that anti-cyclonic motion within the eddy is enhanced by the outward extension, as can be predicted from condition 10). Overall, model results show that the summer condition is favorable to the inward intrusion of the EKWC Water and to the thinning of the UWE.

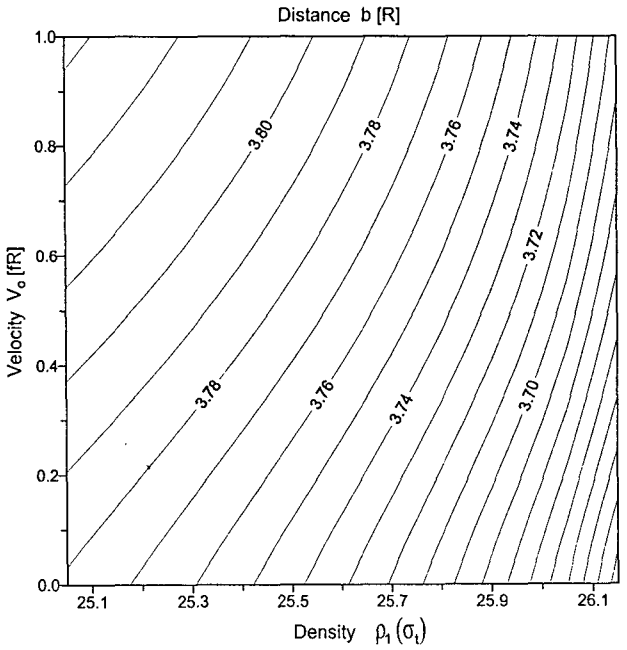

Fig. 9. Distances from the eddy center to the outer edge of the eddy, r=b. Others are the same as in Figure 7.

Discussion and conclusions

It is known by observations that the structure of the UWE undergoes the seasonal change. It has the shape of a warm core ring in early spring after having been renewed by winter convection. As the season progresses toward summer, the upper part of the UWE is affected by the EKWC Water until finally it becomes lens-shaped. A simple analytical model shows that this might be explained by a geostrophic adjustment between the water within the UWE and the surrounding EKWC Water. The inward intrusion of the EKWC Water is mostly favored by the summer condition when the buoyancy of

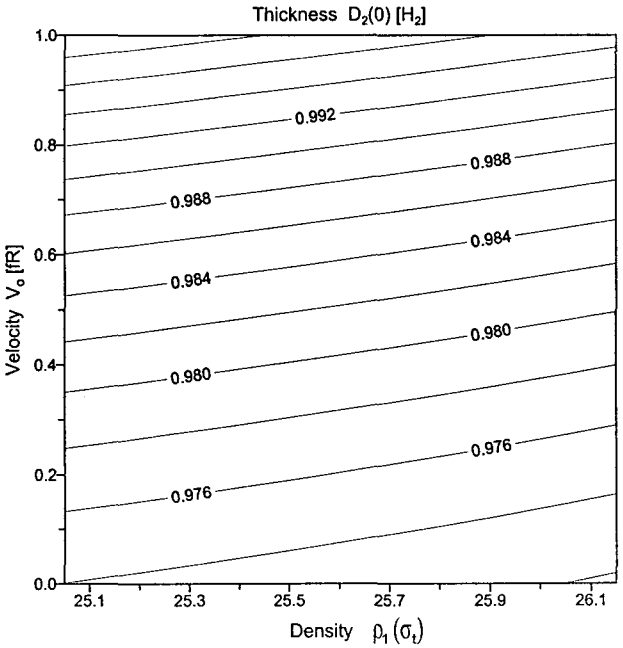

Fig. 10. Thickness of the eddy, D_2, at the eddy center, r=0. Others are the same as in Figure 7.

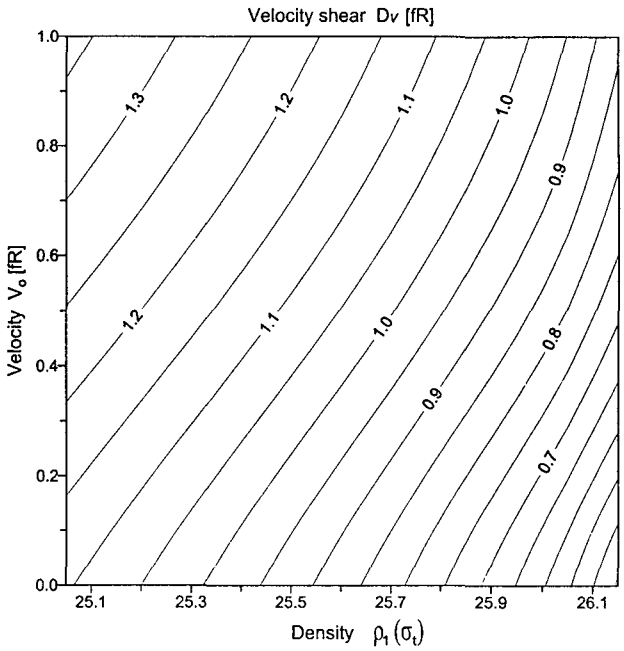

Fig. 11. Maximum velocity difference between the first layer and the eddy, termed velocity shear Dv, which measures the approximate strength of vertical shear between the two layers. Others are the same as in Figure 7.

the EKWC Water increases and the EKWC strengthens.

It should be noted that there may be many other factors affecting the seasonal variation of the UWE, such as eddy-mean current interaction and horizontal or vertical mixing induced either by baroclinic instability or by vertical current shear. Although these problems are beyond the scope of the present study, a discussion on the effect of shear-induced vertical mixing can be given as follows. The model predicts strong vertical shear in the area where the first layer overlies the eddy, which is not clear in the observations (see Fig. 20 or 21 in Shin et al., 1995). The intensity of the vertical shear can be measured by the difference between the maximum cyclonic velocity in the first layer, which occurs at the edge of this layer, r=a, and the maximum anticyclonic velocity in the second layer, which occurs at the outer edge of the eddy, r=b. Indeed, the vertical shear thus estimated appears to increase towards summer (Fig. 11). Vertical turbulence mixing not considered in this model will be enhanced by this vertical shear, resulting in the vertical velocity profile different from that predicted by the model. Likewise, the heat and salt carried by the intrusion of the EKWC Water will be diffused downward by this vertical mixing, hence accelerating the deformation of the UWE. This kind of defect is the weakest part of the model considered. Nevertheless, the model successfully explains the change of eddy shape in terms of the buoyancy and the current speed of the surrounding water, suggesting that the buoyancy increase of the EKWC Water and the strengthening of the EKWC towards summer are largely responsible for the seasonal variation of the UWE.

Acknowledgements

This study was supported by INHA UNIVERSITY Research Grant (INHA-21379). The author thanks Dr. C. Kim of KORDI for providing him necessary data. Comments by anonymous referees were useful in revising the manuscript.

References

Kang, H.-E. and Y.Q. Kang. 1990. Spatio-temporal characteristics of the Ulleung Warm Lens. Bull. Korean Fish. Soc., 23, 407~415.

Kim, C.H. and J.H. Yoon. 1999. A numerical modeling of the upper and intermediate layer circulation in the East Sea. J. Oceanogr., 55, 327~345.

Kim, H.-R. 1991. The vertical structure and temporal variation of the intermediate homogeneous water near Ulleung Island. Master Thesis, Seoul National Univ., 84 pp. (in Korean).

Kim, K.J. and Y.H. Seung. 1999. Formation and movement of the ESIW as modeled by MICOM. J. Oceanogr., 55, 369~382.

Korea Ocean Research and Development Institute. 1993. A study on the meso-scale warm eddy in the southwestern part of the East Sea. KORDI rep., BSPN 00187-611-1, 84 pp. (in Korean).

Korea Ocean Research and Development Institute. 1994. A study on the meso-scale warm eddy in the southwestern part of the East Sea. KORDI rep., BSPN 00222-721-1, 71 pp. (in Korean).

Lie, H.-J., S.-K. Byun, I. Bang and C.-H. Cho. 1995. Physical structure of eddies in the southwestern East Sea. J. Korean Soc. Oceanogr., 30, 170~183.

Moriyasu, S. 1972. The Tsushima Current. In *Kuroshio: Its Physical Aspects*, H. Stommel and K. Yoshida, eds. Univ. of Tokyo Press, Tokyo, pp. 353~369.

Senjyu, T. 1999. The Japan Sea Intermediate Water: Its characteristics and circulation. J. Oceanogr., 55, 111~122.

Seung, Y.H. 1992. A simple model for separation of East Korean Warm Current and formation of North Korean Cold Current. J. Oceanol. Soc. Korea, 27, 189~196.

Seung, Y.H. 1999. A geostrophic adjustment model of shelfward intrusion of oceanic upper water across a depth discontinuity: Implication to the Kuroshio region. Cont. Shelf Res., 19, 247~269.

Seung, Y.H. and K. Kim. 1993. A numerical modeling of the East Sea circulation. J. Oceanol. Soc. Korea, 28, 292~304.

Shin, H.-R., S.-K. Byun, C. Kim, S. Hwang and C.-W. Shin. 1995. The characteristics of structure of warm eddy observed to the northwest of Ulleungdo in 1992. J. Korean Soc. Oceanogr., 30, 39~56 (in Korean).

Uda, M. 1934. The results of simultaneous oceanographical investigations in the Japan Sea and its adjacent waters in May and June 1932. J. Imperial Fish. Exp. St., 5, pp. 138~190 (in Japanese).

Yi, S.-U. 1966. Seasonal and secular variations of the water volume transport across the Korea Strait. J. Oceanol. Soc. Korea, 1, 7~13.

Yoon, J.-H. 1982. Numerical experiment on the circulation in the Japan Sea, Part I: Formation of the East Korean Warm Current. J. Oceanogr. Soc. Japan, 38, 43~51.